Porphyrin Nanostructures

DOI: 10.1002/anie.200806301

Synthesis of Single-Crystal Tetra(4-pyridyl)porphyrin Rectangular Nanotubes in the Vapor Phase**

*Seok Min Yoon, In-Chul Hwang, Kwang S. Kim, and Hee Cheul Choi**

Soft organic nanomaterials have great potential for diverse applications including controlled-release drug delivery,[1] scaffolds for tissue engineering,[2,3] flexible field-effect transistors,[4,5] light-emitting devices, and memory devices[6] on account of their high biocompatibility, optical/electrical properties, and physical flexibility. Among the various candidate unit molecules for organic nanomaterials, porphyrin and its derivatives are of special interest as they possess well-defined π-conjugated electronic systems from chlorophyll units[7] that are exploitable for artificial light harvesting,[8] electronic memory or switch devices, and optical devices.[9,10] Considering that such properties can be tuned by the way in which porphyrin molecules assemble, it may be expected that new or dramatically enhanced properties can be granted by concisely defining the macroscopic structures of porphyrin molecules.

To date, porphyrin derivatives have been synthesized in the form of films,[11,12] nanowheels,[13] nanowires,[14–16] nanobelts,[17,18] and nanotubes[19–21] by various synthetic methods. Among these, 1D porphyrin nanostructures are of special interest, not only because they are beneficial as a smart template for diverse shape-mimicked 1D inorganic nanostructures,[14,20b] but, more importantly, because their electrical and optical properties can be incorporated into viable devices using conventional fabrication processes.[18] Thus, an acquirement of new 1D porphyrin nanostructures alongside the aforementioned structures is desirable for the fundamental understanding of their properties as well as the realization of diverse potential applications. Herein, we report an unprecedented highly crystalline rectangular nanotube (RNT) structure of metal-free 5,10,15,20-tetra(4-pyridyl)porphyrin (H_2TPyP) synthesized by a vaporization–condensation–recrystallization (VCR) process. The VCR process is a modified vapor–solid (VS) process, by which single-crystalline 1D *m*-aminobenzoic acid helical nanobelts and 2D C_{60} nanodisks have been synthesized in high yields.[22,23] The VCR process assures high crystallinity, since it induces recrystallization-based self-assemblies of organic unit molecules with externally provided thermal energy, and avoids the need for solvent molecules.

The formation of H_2TPyP RNTs was initiated by placing H_2TPyP powder in the center of a horizontal furnace heated at 450 °C in an argon atmosphere. The H_2TPyP RNTs formed readily after 30 min on a carbon-coated Si(100) substrate placed at the end region of the furnace, where the temperature had naturally lowered to 350 °C (Figure 1a and Figure S1 in the Supporting Information). For the high-yield synthesis of H_2TPyP-RNTs, the flow rate of Ar gas was set at 100 standard cubic centimeters per minute (sccm). Notably, the H_2TPyP powders started to vaporize at 450 °C, as confirmed by thermogravimetric analysis (TGA, Figure S2 in the Supporting Information). Most of RNTs, which were hollow with rectangular cross-sections, grew vertically against

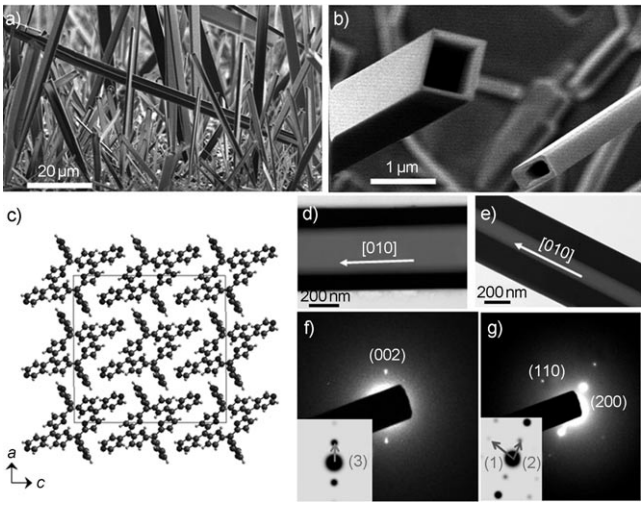

Figure 1. Morphologies and crystal structures of tetra(4-pyridyl)porphyrin rectangular nanotubes (H_2TPyP RNTs). a) Cross-section SEM image of as-grown H_2TPyP RNTs on a carbon-coated Si(100) substrate. b) High magnification SEM image of H_2TPyP RNTs showing hollow spaces with rectangular cross-sections. c) Unit cell of a H_2TPyP RNT. d) and e) TEM images of H_2TPyP RNTs showing (100) and (001) faces, respectively. f) and g) Selected-area electron diffraction (SAED) patterns obtained from (d) and (e), respectively. Insets are corresponding simulated SAED patterns. Arrows 1, 2, and 3 indicate directions from the center (000) to (110), (200), and (002), respectively.

[*] S. M. Yoon, Prof. I. C. Hwang, Prof. K. S. Kim, Prof. H. C. Choi
Department of Chemistry
Pohang University of Science & Technology (POSTECH)
San 31, Hyoja-Dong, Nam-Gu, Pohang (Korea)
Fax: (+82) 54-279-3399
E-mail: choihc@postech.edu

[**] This work was supported by the Nano/Bio Science & Technology Program of MEST (2005-01325), KOSEF through EPB center (R11-2008-052-02000), KOSEF (2008-04306, 2007-8-1158), Korean Research Foundation (MOEHRD, KRF-2005-005J13103), and GRL (KICOS). H.C.C. acknowledges the support from World Class University (WCU) program (R31-2008-000-100059-0). We thank G.-H. Kim, H.-S. Lee at Pohang Accelerator Laboratory 4A Macromolecular Crystallography Wiggler Beamline for data collection, K. S. Jin for TGA, and S. H. Kim for statistical data analysis of H_2TPyP-RNTs.

Supporting information for this article is available on the WWW under http://dx.doi.org/10.1002/anie.200806301.

the substrate surface (Figure 1a and b). The average width, height, and wall thickness of RNTs are approximately 700, 350, and 55 nm, respectively, whereas the length exceeds 10 μm when they are grown under the aforementioned conditions. The population of perfectly square tubes is extremely low, which means that the ratio of height to width for most of the RNTs is greater than one and ranges up to 22, although for roughly 90% of the RNTs, the ratio is between two and four. In addition, the average aspect ratio of length to width is 40, ranging from 2.7 to 500. The RNTs have quite varied widths, heights, and wall thicknesses because they are grown by recrystallization-based self-assembly from their condensates of which sizes are somewhat irregular. However, the overall size of the RNT is controllable to some extent as it is inversely proportional to the flow rate of Ar carrier gas. For example, large H_2TPyP-RNTs, with widths greater than 10 μm and heights greater than 4 μm, are obtained when the flow rate of Ar carrier gas is lowered from 100 to 20–50 sccm.

To investigate the effect of substrates on the growth of H_2TPyP-RNTs, we carried out the reactions on various substrates including glass, hydride-terminated Si(111), highly ordered pyrolytic graphite (HOPG), and carbon-coated Si(100). H_2TPyP RNTs were grown well from all these substrates with the highest yields from carbon-coated Si(100) substrates (Figure S3 in the Supporting Information). The relatively small influence of the substrate indicates that the formation of H_2TPyP condensates does not significantly rely on the types of functional group on the substrate surface, proving that the growth mechanism follows the VCR process. A similar phenomenon was previously observed when *m*-aminobenzoic acid helical nanobelts were formed by the VCR process.[22]

The detail structure of a H_2TPyP RNT was resolved based on single-crystal X-ray diffraction data and selected-area electron diffraction (SAED) patterns. A H_2TPyP RNT, 20 μm in width and 5 μm in height, was examined using a synchrotron X-ray beam source. To avoid twinned diffraction patterns originating from the front and back faces of the RNT, only a single micrometer-scale face of RNT, with 1 μm wall thickness, was prepared by mechanically cutting the RNT along the growth axis. H_2TPyP-RNT has a monoclinic unit cell with $a = 21.042$, $b = 6.888$, and $c = 21.756$ Å and $\beta = 90.37°$ (Figure 1c). The detailed crystal data and results of the structure refinements are summarized in Table S1 in the Supporting Information.

The growth axis of a H_2TPyP RNT was determined from SAED patterns obtained from TEM experiments (Figure 1d–g). As there are two possible faces represented on a TEM grid, that is, wider and narrower faces that correspond to the width and height, respectively, two kinds of SAED patterns, corresponding to [100] and [001] zone axes, could be indexed. The experimentally obtained SAED patterns matched well with simulated ones (inset images in Figure 1f and g),[24] as their distance ratios of (110):(200):(002) and (1):(2):(3) are identical and the angle of (110)-(000)-(002) is equal to (1)-(000)-(2). Since the ratio of width to height is greater than one, the probability of the H_2TPyP RNT lying on a wider face is higher when samples are randomly deposited on a copper TEM grid, which should result in more frequent findings of SAED patterns from the H_2TPyP RNTs laid down on a wider face. Indeed, similar SAED patterns to that in Figure 1f were observed for more than 90% of independently prepared samples. Consequently, it can be concluded that the wider face is (100), the narrower one is (001), and the growth axis of H_2TPyP RNTs is [010].

Based on the unit cell, growth axis, and crystallographic planes of each face, a H_2TPyP RNT model was constructed by systematically packing the unit cells into three axes. Owing to the computation power limit, a model representing a miniaturized RNT, 30 nm in width, 16 nm in height, and 2.1 nm in wall thickness, was built up (Figure 2b).[25] This model

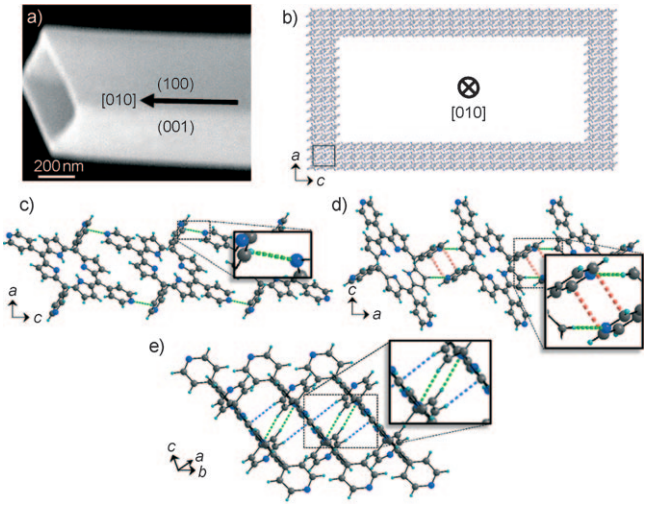

Figure 2. a) SEM image of a H_2TPyP RNT. b) Model of a H_2TPyP RNT built up with 420 unit cells according to the ratio of wall thickness, width, and height of the H_2TPyP RNT shown in (a); 15 along the *c* axis, 8 along the *a* axis, and 10 along the *b* axis. A black box in the bottom-left corner indicates a unit cell of a H_2TPyP RNT. c)–e) Self-assembled H_2TPyP molecules along the *c* (width), *a* (height), and *b* (length) axes, respectively. C gray; H pale blue; N blue. The green, blue, and red dotted lines indicate hydrogen-bonding, hydrogen–π, and π–π intermolecular interactions, respectively.

matches the dimension ratio of an experimentally obtained H_2TPyP RNT (Figure 2a). The key driving forces for the growth of self-stacking unit cells into a rectangular tubular structure are three intermolecular interactions independently applied along the *c*, *a*, and *b* axes: 1) Packing of H_2TPyP molecules along the *c* axis (width) involves hydrogen-bonding interactions between a hydrogen atom and a nitrogen atom of two pyridyl groups (N–H 2.662 Å; Figure 2c). 2) Packing of H_2TPyP molecules along the *a* axis (height) involves hydrogen bonding (N–H 2.429 Å) and a displaced π–π stacking interaction (centroid–centroid 3.385 Å) among four π electrons in pyridyl rings (Figure 2d). 3) Along the *b* axis (length), two intermolecular interactions influence the packing: hydrogen bonding between a hydrogen atom in the pyridyl group and a nitrogen atom in the core part of H_2TPyP molecules (N–H 2.671 Å), and a hydrogen–π intermolecular interaction between a hydrogen atom in the pyridyl group and π electrons on a carbon atom in the core part of H_2TPyP (H–π 2.803 Å; Figure 2e).

To investigate the mechanism of the formation of hollow space in H_2TPyP RNTs, the growths of RNTs was examined at various reaction times (Figure 3). At the earliest stage of the VCR process, two minutes after the vaporization temperature reached 450 °C, H_2TPyP condensates of various sizes were found on the substrate, none of which were RNTs. The substrate temperature at this point was 350 °C. After a further five minutes reaction time, vertically grown H_2TPyP rods has formed, implying that the growth of H_2TPyP RNTs originates from its rod form. After 10–30 minutes, half-filled and half-tubular structures were formed. Such rod–tube heterostructures are a result of the uneven adsorption rate of H_2TPyP monomers on the outside and inside of the rod, resulting in the growth of thin walls to form tubes at a higher rate than the piling rate to form rods. The tube/rod length ratio became significantly higher after 30 minutes, yielding a high population of H_2TPyP RNTs. Under the conventional reaction conditions, the average yields of RNTs and rods are 65% and 35%, respectively, as determined using an inverted optical microscope in bright fields. Such a preferred adsorption of precursor molecules on the edge of a growing nanostructure is energetically favorable[26] and has been considered a key mechanism supporting the formation of iridium nitride nanotubes[27] and tellurium tubular structures.[28]

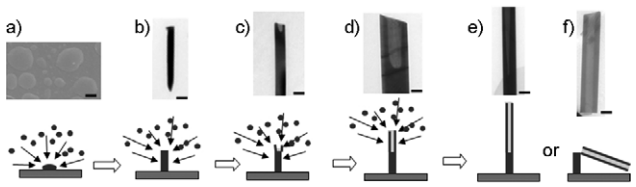

Figure 3. Transformation of morphology of H_2TPyP RNT from condensates, through rod shape, to hollow tubular structures. a) Morphologies of H_2TPyP condensates after reaction for 2 min; b) 5 min; c) 10 min; d) 15 min; e, f) 30 min after the reaction temperature reaches 450 °C. The scale bars indicate 1.5 μm.

In summary, H_2TPyP molecules were selectively grown into single-crystalline rectangular nanotube (RNT) structures by the VCR process. The systematic assembly of H_2TPyP molecules into three axes, induced by hydrogen bonding, hydrogen–π interactions, and π–π interactions,[29] results in the formation of rod structures at an early stage, and eventually to rectangular tubular structures at later growth stages. Whereas previously reported 1D porphyrin nanostructures are composed of metalloporphyrins, non-metalloporphyrin H_2TPyP RNTs are especially attractive for the radical tuning of their electrical and optical properties, since the empty metal sites can be simply tailored with various metal ion species by simple post-treatments, such as ion-exchange,[30–32] or by cocrystallization with functional compounds.[33–35] We also believe that H_2TPyP RNTs may lead to the development of new sub-micrometer-scale organic optoelectronic devices, with both optical cavities and electron-transport capabilities.[36]

Experimental Section

Synthesis of tetra(4-pyridyl)porphyrin rectangular nanotubes (H_2TPyP RNTs): 5,10,15,20-Tetra(4-pyridyl)porphyrin (H_2TPyP, 97%) was purchased from Sigma–Aldrich. H_2TPyP powder (0.04 g, 0.065 mmol) was placed in the middle of quartz tube, with solid substrates located at the end region of the tube. The tube was then placed in a horizontal tube furnace system (Figure S1 in Supporting Information). Prior to reaction, the inner atmosphere of the quartz tube was flushed with pure Ar gas (99.999%) at a flow rate of 100 sccm. Under the Ar atmosphere, the quartz tube was heated from room temperature to 450 °C at a rate of 61 °C min^{-1} and maintained at 450 °C for 40 min.

Characterization: The morphologies, product yields, and the growth axis were characterized by scanning electron microscopy (SEM, FEI XL30S) and transmission electron microscopy (TEM, Philips CM200). Au was sputtered on H_2TPyP RNT samples for SEM measurements. Samples for TEM studies were prepared by soaking original substrates containing as-grown H_2TPyP RNTs in water to remove them from the substrates. The RNTs floating on the water surface were then transferred onto carbon-coated copper grids using a glass pipette. Thermogravimetric analysis (TGA) measurements were carried out using a Seiko TG/DT analyzer (Model EXSTAR 6000 TG/DT, Tokyo, Japan). For TGA experiments, samples were loaded into an aluminum pan and heated from room temperature to 800 °C at a rate of 10 °C min^{-1}.

X-ray crystal structure determination: X-ray diffraction data of H_2TPyP RNT were collected from a single H_2TPyP RNT, 30 μm in width and 10 μm in depth, at 190 K. A synchrotron radiation ($\lambda = 0.75000$ Å) source was equipped with an ADSC Quantum 210 CCD diffractometer at the Macromolecular Crystallography Wiggler Beamline 4A, Pohang Accelerator Laboratory (PAL), Pohang, Korea. Data reduction and adsorption correction were carried out using the HKL2000 programs.[37] The Bruker SHELXL programs were used for structure solution and refinement.[38,39]

Received: December 24, 2008
Published online: February 20, 2009

Keywords: crystal growth · nanostructures · nanotubes · porphyrin · self-assembly

[1] B. J. Jeong, Y. H. Bae, D. S. Lee, S. W. Kim, *Nature* **1997**, *388*, 860–862.
[2] K. Y. Lee, D. J. Mooney, *Chem. Rev.* **2001**, *101*, 1869–1879.
[3] a) C. Czeisler, K. L. Niece, E. Beniash, D. A. Harrington, J. A. Kessler, S. I. Stupp, *Science* **2004**, *303*, 1352–1355; b) S. I. Stupp, *MRS Bull.* **2005**, *30*, 546–552; c) K. Rajangam, H. A. Behanna, M. J. Hui, X. Han, J. F. Hulvat, J. W. Lomasney, S. I. Stupp, *Nano Lett.* **2006**, *6*, 2086–2090.
[4] Y. Y. Lin, D. J. Gundlach, S. F. Nelson, T. N. Jackson, *IEEE Electron Device Lett.* **1997**, *18*, 606–608.
[5] C. D. Dimitrakopoulos, S. Purushothaman, J. Kymissis, A. Callegari, J. M. Shaw, *Science* **1999**, *283*, 822–824.
[6] S. Möller, C. Perlov, W. Jackson, C. Taussig, S. R. Forrest, *Nature* **2003**, *426*, 166–169.
[7] B. J. van Rossum, D. B. Steensgaard, F. M. Mulder, G. J. Boender, K. Schaffner, A. R. Holzwarth, H. J. M. de Groot, *Biochemistry* **2001**, *40*, 1587–1595.
[8] D. Gust, T. A. Moore, A. L. Moore, *Acc. Chem. Res.* **2001**, *34*, 40–48.
[9] N. R. J. Armstrong, *J. Porphyrins Phthalocyanines* **2000**, *4*, 414–416.
[10] R. W. Wagner, S. J. Lindsey, J. Seth, V. Palniappan, D. F. Bocian, *J. Am. Chem. Soc.* **1996**, *118*, 3996–3997.

[11] C. D. Dimitrakopoulos, P. R. L. Malenfant, *Adv. Mater.* **2002**, *14*, 99 – 117.
[12] L. Li, Q. Tang, H. Li, X. Yang, W. Hu, Y. Song, Z. Shuai, W. Xu, Y. Liu, D. Zhu, *Adv. Mater.* **2007**, *19*, 2613 – 2617.
[13] J. Hofkens, L. Latterini, P. Vanoppen, H. Faes, K. Jeuris, S. D. Feyter, J. Kerimo, P. F. Barbara, F. C. De Schryver, A. E. Rowan, R. J. M. Nolte, *J. Phys. Chem. B* **1997**, *101*, 10588 – 10598.
[14] Z. Wang, K. J. Ho, C. J. Medforth, J. A. Shelnutt, *Adv. Mater.* **2006**, *18*, 2557 – 2560.
[15] A. D. Schwab, E. Smith, B. Bond-Watts, D. E. Johnston, J. Hone, A. T. Johnson, J. C. de Paula, W. F. Smith, *Nano Lett.* **2004**, *4*, 1261 – 1265.
[16] B. N. Mbenkum, E. Barrena, X. Zhang, M. Kelsch, H. Dosch, *Nano Lett.* **2006**, *6*, 2852 – 2855.
[17] W. Y. Tong, A. B. Djurišić, M. H. Xie, A. C. M. Ng, K. Y. Cheung, W. K. Chan, Y. H. Leung, H. W. Lin, S. Gwo, *J. Phys. Chem. B* **2006**, *110*, 17406 – 17413.
[18] a) Q. Tang, H. Li, M. He, W. Hu, C. Liu, K. Chen, C. Wang, Y. Liu, D. Zhu, *Adv. Mater.* **2006**, *18*, 65 – 68; b) Q. Tang, H. Li, Y. Liu, W. Hu, *J. Am. Chem. Soc.* **2006**, *128*, 14634 – 14639.
[19] J. S. Hu, Y. G. Guo, H. P. Liang, L. J. Wan, L. Jiang, *J. Am. Chem. Soc.* **2005**, *127*, 17090 – 17095.
[20] a) Z. Wang, C. J. Medforth, J. A. Shelnutt, *J. Am. Chem. Soc.* **2004**, *126*, 15954 – 15955; b) Z. Wang, C. J. Medforth, J. A. Shelnutt, *J. Am. Chem. Soc.* **2004**, *126*, 16720 – 16721.
[21] T. Kojima, R. Harada, T. Nakanish, K. Kaneko, S. Fukuzumi, *Chem. Mater.* **2007**, *19*, 51 – 58.
[22] S. M. Yoon, I. C. Hwang, N. Shin, D. Ahn, S. J. Lee, J. Y. Lee, H. C. Choi, *Langmuir* **2007**, *23*, 11875 – 11882.
[23] H. S. Shin, S. M. Yoon, Q. Tang, B. Chon, T. Joo, H. C. Choi, *Angew. Chem.* **2008**, *120*, 705 – 708; *Angew. Chem. Int. Ed.* **2008**, *47*, 693 – 696.
[24] Single crystal 1.0.0. Crystal Maker Software Ltd.
[25] Diamond 3.1e. Crystal Impact GbR.
[26] G. C. Krueger, C. W. Miller, *J. Chem. Phys.* **1953**, *21*, 2018 – 2023.
[27] L. W. Yin, Y. Bando, D. Golberg, M. S. Li, *Adv. Mater.* **2004**, *16*, 1833 – 1838.
[28] B. Mayers, Y. Xia, *Adv. Mater.* **2002**, *14*, 279 – 282.
[29] K. S. Kim, P. Tarakeshwar, J. Y. Lee, *Chem. Rev.* **2000**, *100*, 4145 – 4185.
[30] L. Pan, B. C. Noll, X. Wang, *Chem. Commun.* **1999**, 157 – 158.
[31] L. Carlucci, G. Ciani, D. M. Proserpio, F. Porta, *Angew. Chem.* **2003**, *115*, 331 – 336; *Angew. Chem. Int. Ed.* **2003**, *42*, 317 – 322.
[32] L. L. Li, C. J. Yang, W. H. Chen, K. J. Lin, *Angew. Chem.* **2003**, *115*, 1543 – 1546; *Angew. Chem. Int. Ed.* **2003**, *42*, 1505 – 1508.
[33] D. Sun, F. S. Tham, C. A. Reed, P. D. W. Boyd, *Proc. Natl. Acad. Sci. USA* **2002**, *99*, 5088 – 5092.
[34] K. Kumar, I. Goldberg, *Angew. Chem.* **1998**, *110*, 3176 – 3180; *Angew. Chem. Int. Ed.* **1998**, *37*, 3027 – 3030.
[35] S. Anderson, H. L. Anderson, A. Bashall, M. McPartlin, J. K. M. Sanders, *Angew. Chem.* **1995**, *107*, 1196 – 1200; *Angew. Chem. Int. Ed.* **1995**, *34*, 1096 – 1099.
[36] K. Yamashita, Y. Matsumura, Y. Harima, S. Miura, H. Suzuki, *Chem. Lett.* **1984**, 489 – 492.
[37] Z. Otwinowski, W. Minor, *Methods Enzymol.* **1997**, *276*, 307 – 326.
[38] G. Sheldrick, Program for Crystal Structure Solution, Universität Göttingen, **1986**.
[39] G. Sheldrick, Program for Crystal Structure Refinement, Universität Göttingen, **1993**.

